Comparative Characterization Study of Microporous Carbons by HRTEM Image Analysis and Gas Adsorption

D. Lozano-Castello,*,† D. Cazorla-Amoros,† A. Linares-Solano,† K. Oshida,‡ T. Miyazaki,‡ Y. J. Kim,§ T. Hayashi,§ and M. Endo§

Departamento de Quimica Inorganica, Universidad de Alicante, E-03080, Alicante, Spain, Nagano National College of Technology, 716 Tokuma, Nagano-shi, 381-8550, Japan, and Faculty of Engineering, Shinshu University, 4-17-1 Wakasato, Nagano 380-8553, Japan

Received: April 14, 2005; In Final Form: June 10, 2005

The present work presents a useful comparison of micropore size distributions (MPSDs) obtained from gas adsorption and image analysis of high-resolution transmission electron micrographs. It is shown that the MPSD obtained for a chemical activated carbon is concordant with that obtained from CO_2 adsorption. In addition, this technique has allowed us to obtain the MPSD of a carbon molecular sieve (CMS) prepared in our laboratory by a copyrolysis process, which could only be characterized by CO_2 adsorption at 273 K (not by N_2 adsorption at 77 K due to diffusional problems). The MPSD obtained by high-resolution transmission electron microscopy (HRTEM) for the CMS is wider than that obtained by CO_2 adsorption, suggesting that HRTEM is detecting the closed porosity existing in this sample, which is not accessible to gas adsorption. The existence of closed porosity in the CMS is explained considering the preparation method used. Thus, HRTEM combined with image analysis seems to be useful for structural analysis of narrow micropores including closed porosity.

Introduction

Porous carbons, such as activated carbons (ACs), activated carbon fibers (ACFs), and carbon molecular sieves (CMSs), are being used in many different application fields such as antipollution systems (i.e., water purification, abatement of volatile organic compounds, selective remove of SO_x/NO_x, etc.), energy devices (electric double layer capacitors for electronics and electric vehicles), and gas separation because of their high specific surface areas (SSAs) and pore structures. From this high potential in various applications, numerous scientists have been devoted to clarify the pore structure of these materials with diverse methods. Characterization in terms of the pore size distribution (PSD) is indispensable for the utilization and tailoring of improved carbon materials in those and many other applications. In general, pore analysis techniques based on gas adsorption methods have been well developed and quite successfully applied to characterize porous carbons, allowing the obtaining of quite reasonable micropore size distributions (MPSDs).

Among gas adsorption techniques, nitrogen adsorption is the most widely used technique due to its considerable sensitivity to both the micropore and mesopore regimes. However, when it is used for the characterization of microporous solids, diffusional problems of the molecules inside the narrow porosity range (size <0.7 nm) occur, especially for CMSs. To overcome this problem, the use of other adsorptives is necessary, such as CO_2 adsorption at 273 K.[1−4] In a previous work,[5] the micropore size distributions (MPSDs) of two activated carbons and a carbon molecular sieve (CMS) were assessed by high-pressure methane and carbon dioxide adsorption isotherms. The results showed a quite good consistency between both gases, despite the different gas characteristics (CH_4 and CO_2) and adsorption conditions (298 K, supercritical conditions, and 273 K, subcritical conditions, respectively). Although the usefulness of CO_2 adsorption has been the object of intensive debates,[1−5] its use is not generalized. To strengthen the importance of the results obtained with CO_2 adsorption data, complementary techniques other than gas adsorption are required. In this sense, small-angle X-ray scattering (SAXS) and μSAXS techniques were used in previous work.[6−8] However, other independent techniques are still needed to confirm the usefulness of CO_2 adsorption.

In recent works[9−11] PSDs of ACs and ACFs were obtained using image analysis of micrographs obtained from high-resolution transmission electron microscopy (HRTEM). The results obtained suggested that the method could be a powerful and useful tool to characterize porous materials. Thus, the objective of the present work is to obtain MPSDs by use of the HRTEM technique and to compare these MPSDs with those determined with more established techniques, such as gas adsorption. It should be remarked that a comparative study of the results obtained by HRTEM image analysis and by N_2 adsorption at 77 K in ACF was carried out in a previous work.[9] That study showed a good fitting of both results in the mesopore region (2−50 nm) and in the micropore range wider than 1.5 nm. Thus, in the present work the micropore region and especially the small micropore region (ultramicropore, pore size <0.7 nm, approximately) are analyzed by HRTEM image analysis. For such a purpose, two microporous activated carbons and a carbon molecular sieve, which were characterized in detail by high-pressure CO_2 and CH_4 adsorption in a previous work,[5] were selected.

Considering that HRTEM images depend on the phase contrast transfer function of the objective lens of the HRTEM

* Corresponding author. Fax: (34) 965 90 3454. E-mail: d.lozano@ua.es.
† Universidad de Alicante.
‡ Nagano National College of Technology.
§ Shinshu University.

10.1021/jp051928m CCC: $30.25
Published on Web 07/19/2005

TABLE 1: Porous Texture Characterization Results Obtained from N_2 (77 K) and CO_2 (273 K) Adsorption Data

sample	BET surf. area (m^2/g)	$V(N_2)$ (cm^3/g)	$V(CO_2)$ (cm^3/g)
KUA1B8			0.20
KUA1GC	2021	0.83	0.80
KUA1L26	3290	1.45	0.81

(hereinafter referred to as the transfer function), the transfer function must be comprehended for exact observation of amorphous structured materials such as activated carbons. Thus, in the present study amorphous carbon films with HRTEM on different defocus values (Δf) are observed in order to determine the transfer function of the HRTEM as well as simulation of the transfer function. Power spectra of the HRTEM images of the amorphous carbon film obtained by two-dimensional (2D) fast Fourier transform (FFT) are compared to the simulation data.

Thus, the objectives of this work are (i) to reinforce the use of CO_2 with an independent technique (HRTEM) and (ii) to confirm the usefulness of HRTEM with gas adsorption.

Experimental Section

The series of activated carbons includes the following: (i) a carbon molecular sieve (sample KUA1B8) prepared at the University of Alicante by blocking the microporosity of a previously prepared activated carbon (KUA1GC) by cracking hydrocarbons;[12] (ii) two activated carbons prepared by chemical activation with KOH of a Spanish anthracite (KUA1GC and KUA1L26).[13]

Porous texture analysis of all the samples was carried out by subatmospheric N_2 and CO_2 adsorption at 77 and 273 K, respectively, in a Micromeritics (ASAP 2010, Micromeritics, USA) instrument. Table 1 contains the BET surface areas and micropore volumes obtained by applying the Dubinin−Radushkevich (DR) equation to the N_2 and CO_2 adsorption isotherms at 77 and 273 K, respectively. CO_2 and CH_4 adsorption isotherms at 273 and 298 K, respectively, and at high pressures (up to 4 MPa) were obtained in a Sartorius high-pressure microbalance. More details can be found elsewhere.[1,2]

Determination of the Transfer Function of the HRTEM. A 200 kV acceleration voltage HRTEM (JEOL 2010FEF, field emission type) was used. Considering that the transfer function must be comprehended for exact observation of amorphous structured materials such as AC, an amorphous carbon film of supporting lamella of TEM grid was observed by the HRTEM under some different underfocus values (Δf's) to determine the transfer function of the HRTEM. A CCD camera, which is equipped in the HRTEM, was used for observation to obtain a linear brightness image in the intensity of electron beam. Power spectra of the HRTEM images of amorphous carbon film were obtained by 2D-FFT.[14,15] The power spectra are represented by graphs by integration of rotative direction around their center points. The power spectra are compared to the effective transfer functions of the HRTEM. To calculate the effective transfer function, the transfer function $\cos(\chi)$ of the HRTEM was obtained by the following equation:[16]

$$\cos(\chi) = \cos\left[\frac{\pi}{2} - \frac{2\pi}{\lambda}C_s\frac{(2\theta)^4}{4} + \frac{2\pi}{\lambda}\Delta f\frac{(2\theta)^2}{2}\right] \qquad (1)$$

θ is the Bragg angle, C_s is the spherical aberration constant of the lens, Δf is the underfocus value, and λ is the de Broglie wavelength of the electrons. C_s of JEOL 2010FEF is 1.6 mm, and λ is 0.002 508 nm when the acceleration voltage is 200 kV. Considering that the resolution of the HRTEM is limited by the special coherence of the electron beam and by chromatic effects, an effective transfer function was obtained by multiplying a damping curve of these effects on the transfer function.

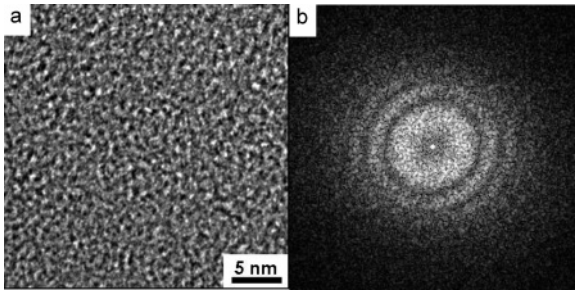

Figure 1. (a) HRTEM image of amorphous carbon film and (b) power spectrum of (a) obtained by 2D-FFT. The defocus value Δf is −255 nm.

Determination of MPSDs by HRTEM. MPSDs of samples were calculated by means of image analysis of HRTEM micrographs. Samples were inserted in a glass tube filled with ethanol, and they were dispersed by ultrasonic waves. Samples dispersed in methanol were mounted on the microgrid for TEM observation by surface tension several times. The microgrid was dried for about 3 h. Observation was performed from low magnification to high magnification by HRTEM (JEOL 2010FEF, field emission type). The TEM image obtained at 200000× magnification ($\Delta f = -60$ nm) was converted to a 512 × 512 pixel, 8 bits gray scale image to perform the two-dimensional fast Fourier transform (2D-FFT). The resultant 2D power spectrum confirmed the isotropy of the specimen. The strength of the 2D power spectrum around the concentric circles that were centered at the center of the image was integrated to get the one-dimensional (1D) integrated spectra. The 1D integrated spectrum had pore diameters preferentially aligned along the *x*-axis, and the intensity of each value is evaluated along the *y*-axis, to obtain the PSD.

Results and Discussion

Determination of Transfer Function of the HRTEM. An HRTEM image of amorphous carbon film of TEM grid is shown in Figure 1a. The defocus value Δf of the image is selected to be −255 nm because peaks of the power spectrum obtained by 2D-FFT are well indicated with the large declination from the just focus. The power spectrum of Figure 1a shown in Figure 1b was obtained by 2D-FFT.

To remove the effect of discontinuity of the image edges, the window treatment was performed on the HRTEM image (Figure 1a) before the 2D-FFT operation.[17] The components of the spectrum are distributed concentrically. The symmetric property of the center point of the power spectrum indicates the isotropic structure of the amorphous carbon film.

The power spectrum (Figure 1b) was transformed into the graph shown in Figure 2a by integration of rotative direction around its center points. The angle of 180° is enough as the integration angle since the power spectrum is symmetric with respect to the center point. The integration data were divided by the distance from the center point to make a one-dimensional graph. The virtual axis of Figure 2a shows the intensity of the integrated spectrum; the spectrum is shown in logarithmic scale. The space frequency is transferred to the space wavelength on the horizontal axis. The transfer function at $\Delta f = -255$ nm is shown in Figure 2b. The curve L_1 is the transfer function without damping calculated by eq 1. The curves L_2 show the damping envelope function. The curve L_3 is an effective transfer function

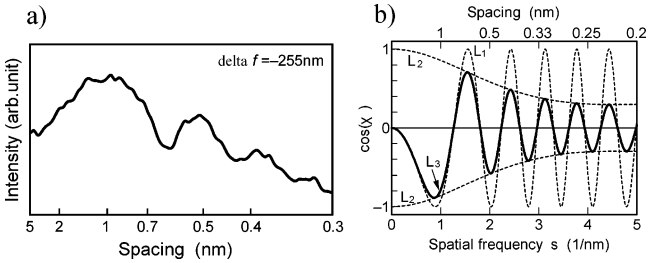

Figure 2. (a) Power spectrum of HRTEM image of amorphous carbon film obtained by 2D-FFT. (b) Phase transfer function of objective lens of the HRTEM. The defocus value Δf is −255 nm. L_1, transfer function without attenuation obtained by eq 1; L_2, damping envelope curves; L_3, effective transfer function modified by the damping envelope function.

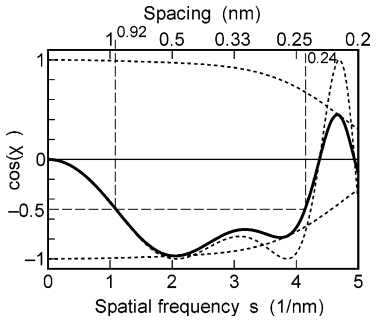

Figure 3. Phase transfer function of objective lens of the HRTEM at defocus value $\Delta f = -60$ nm. L_1, transfer function without attenuation obtained by eq 1; L_2, damping envelope curves; L_3, effective transfer function modified by the damping envelope function.

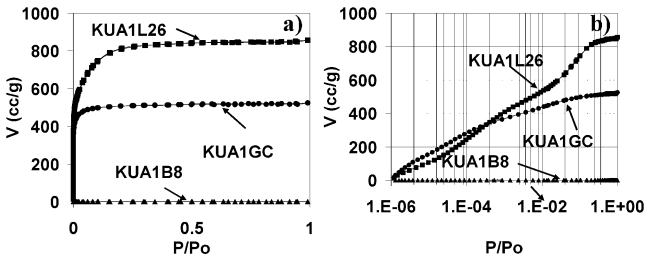

Figure 4. Nitrogen adsorption−desorption isotherms at 77 K. (a) Linear scale on abscissa and (b) logarithmic scale on abscissa.

which was obtained by imposing the envelope function L_2 on the transfer function L_1. The positions of peaks of the power spectrum on the horizontal axis (Figure 2a) approximately equal the positions of underpeaks of the transfer function (Figure 2b). It is shown that the transfer function is calculated correctly. The same HRTEM observation and calculation of the transfer function were carried out at different defocus values from −60 to −510 nm, and verified.

The optimum Δf "Scherzer focus" of the HRTEM is 60 nm obtained by the equation of $1.2(C_s\lambda)^{1/2}$ nm. Figure 3 shows the phase transfer function at $\Delta f = -60$ nm, which was calculated like that of Figure 2b. The HRTEM image has a good contrast when the absolute value of the transfer function is larger than 0.5. Thus, the transfer function in Figure 3 shows that a good contrast of the HRTEM image is obtained in the range from 0.24 to 0.92 nm, which is indicated by dashed lines.

Determination of MPSD by HRTEM and Its Comparison with Gas Adsorption. Figure 4a presents the N_2 adsorption−desorption isotherms at 77 K corresponding to the activated carbons. The adsorption for the carbon molecular sieve (sample KUA1B8) was negligible because this sample presents a very narrow microporosity, not accessible to N_2 at 77 K.[1,2] The kinetics of N_2 adsorption is extremely slow at 77 K. Nitrogen adsorption

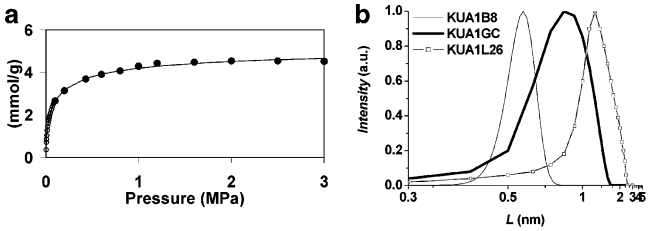

Figure 5. (a) CO_2 adsorption isotherm at 273 K corresponding to carbon molecular sieve (sample KUA1B8). (b) Normalized MPSD obtained from the CO_2 adsorption data (subatmospheric and high-pressure adsorption data) for the three samples used in the present study.

isotherms obtained for the others are of type I, indicating the presence of only micropores.

Considering the curvature radius of the knee of the isotherm before reaching the saturation plateau, each sample can be clearly distinguished: KUA1GC shows very a sharp knee compared to those of the others and KUA1L26 has the largest adsorption capacity. These detailed adsorption behaviors in low relative pressure are presented in a logarithm scale in Figure 4b. It is worth noting that the amount of nitrogen adsorbed by KUA1GC at very low pressure is higher than that for the other samples, even though it shows a lower adsorption capacity at the high relative pressure range. Considering that, in the low-pressure region, the adsorption capacity of porous materials with narrow micropores is high due to the enhanced molecule−surface interaction, the high adsorption at low relative pressure of the sample KUA1GC implies that the porosity of this sample has an important contribution from narrow micropores. From these adsorption isotherms, no information about the pore texture of sample KUA1B8 (a carbon molecular sieve) can be obtained due to the too narrow pore size of this sample.

To get information about sample KUA1B8, CO_2 adsorption isotherms at 273 K (subatmospheric and high-pressure adsorption) were carried out for the three samples. As an example, Figure 5a presents the CO_2 adsorption isotherm at 273 K corresponding to sample KUA1B8, which could not be characterized by N_2 adsorption at 77 K. The CO_2 isotherm is of type I, characteristic of a microporous material. It has a sharp knee, reaching the plateau at low pressure. This suggests that this sample has a narrow micropore size distribution (MPSD). From the CO_2 adsorption isotherms, MPSDs for the three samples were calculated (see Figure 5b). A detailed description of the method used to obtain these MPSDs can be found elsewhere.[5] To make easier the comparison with TEM data, which will be presented later, the MPSD curves from CO_2 adsorption data have been normalized to the maximum of each curve. It can be seen that, as expected from the preparation method used, the narrowest MPSDs correspond to the carbon molecular sieve (sample KUA1B8), which presents a very homogeneous porosity. Sample KUA1GC also has a quite narrow MPSD, although the mean pore size is shifted to higher values. Sample KUA1L26 has a wider MPSD with a higher mean pore size.

Figure 6 shows high-resolution TEM images taken at a magnification of 200000× and the power spectra obtained by carrying out a 2D-FFT of original images corresponding to the three samples. The defocus value Δf was −60 nm. In the TEM images, the bright sections are considered as pores, which was confirmed by TEM image simulation.[9] We have confirmed that there is no abrupt structural change, which can affect the results of pore size distribution by image analysis by varying the observation place from part to part. Furthermore, overall structures of samples were also observed. All samples show

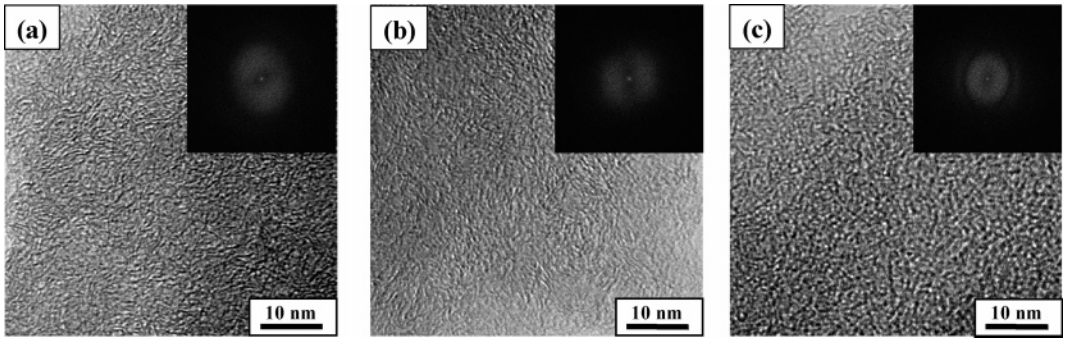

Figure 6. High-resolution TEM photographs and power spectra (insets) obtained from fast Fourier transform. (a) KUA1B8; (b) KUA1GC; (c) KUA1L26.

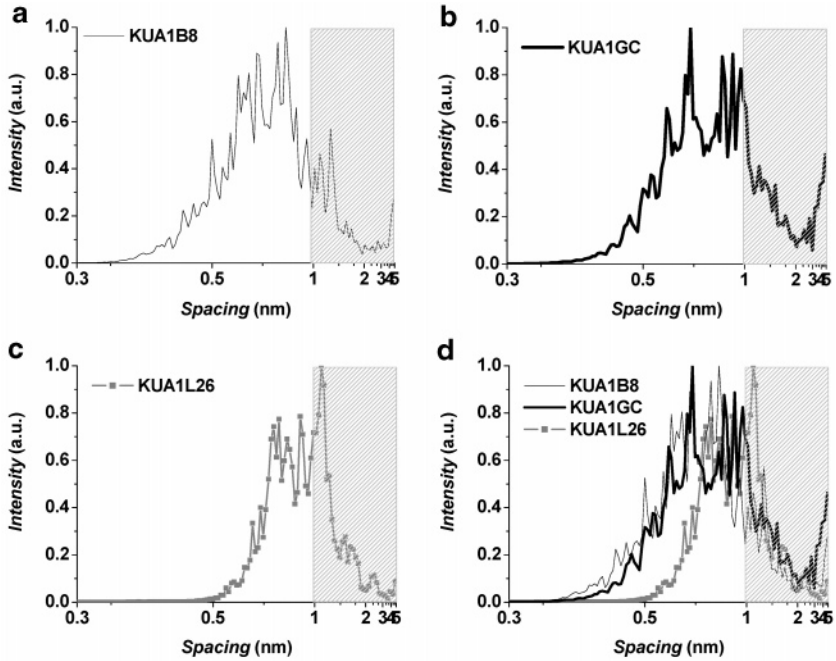

Figure 7. Micropore size distributions obtained by image analysis using HRTEM photographs corresponding to samples (a) KUA1B8, (b) KUA1GC, and (c) KUA1L26; (d) comparison among the three samples.

very complex pore configurations, having various dimensions and irregular shapes. Considering the observation range of good contrast (from 0.24 to 0.92 nm), the ultramicropores (pore size <0.7 nm, approximately) must appear in Figure 6.

In Figure 7, MPSDs obtained by integration around the center point of the power spectrum are presented. The abscissa, denoted as spacing, corresponds to the pore size, which contains the thickness of the pore wall, and the ordinate implies the intensity with arbitrary units. The MPSDs in Figure 7 were obtained by normalizing each curve to the maximum of each profile. Therefore, intensity in this MPSD can hardly be used as an absolute value such as adsorption amount in gas adsorption methods. In these results, only the peak location and relative intensity are considered. As discussed in the previous section, the range for good contrast is from 0.24 to 0.92 nm, which is shown in Figure 7, except in the hatched area.

Figure 7a presents the MPSD corresponding to the carbon molecular sieve (sample KUA1B8). According to this result most of the porosity of this sample is narrow microporosity (pore size below 0.8 nm approximately), which agrees with the molecular sieve properties of this sample. It must be remarked that the narrow porosity existing in this sample, which could be characterized not by N_2 adsorption at 77 K, but with CO_2 adsorption at 273 K, has been analyzed by image analysis. A comparison of this MPSD with the curve presented in Figure 5 indicates that the MPSD obtained for this sample by this technique is wider than that obtained for the same sample by CO_2 adsorption (Figure 5). This fact could be explained if we assume that HRTEM is detecting closed porosity, existing in sample KUA1B8, which is not accessible to CO_2 adsorption.

The existence of closed porosity in sample KUA1B8 can be justified if we consider the process used for the preparation of this sample. As briefly explained in the Experimental Section and in more detail in a previous work,[12] sample KUA1B8 has been prepared by a copyrolysis process, where the porosity of sample KUA1GC was partially blocked by cracking hydrocarbons evolved by a coal tar pitch. From the porous texture characterization results of both samples (KUA1B8 and KUA1GC) (see Table 1), it is observed that after the cracking process there is a reduction in the narrow micropore volume of 0.6 cm^3/g. The weight percentage of carbon deposition in this sample was 49%. In the case that the reduction of 0.6 cm^3/g in the micropore volume would be due to the filling of this micropore volume with carbon, the weight percentage of carbon deposition would be 130%, instead of 49%. The fact that the weight percentage of carbon deposition is much less than 130% confirms that, during the copyrolysis process, carbon deposition takes place mainly in the external part of the pores, reducing the pore size, and blocking part of the starting porosity of the activated carbon

precursor, so that the internal porosity of the CMS, not accessible to gas adsorption, seems to be observed by HRTEM.

The MPSDs corresponding to the two activated carbons (KUA1GC and KUA1L26) are presented in parts b and c, respectively, of Figure 7. It can be seen that, in the case of sample KUA1GC, the MPSD obtained with this technique is quite concordant with that obtained with CO_2 adsorption (Figure 5). This similarity is noteworthy, taking into account that the techniques are very different. In the case of sample KUA1L26, the MPSD is shifted to wider mean pore sizes compared to those of sample KUA1GC, which agrees with CO_2 adsorption results. Considering that the MPSD obtained for this sample is mostly located in the region where the contrast is not good, the results corresponding to this sample will not be discussed in detail in this paper.

For comparison purposes, Figure 7d includes the MPSDs obtained for the three samples. Samples KUA1B8 and KUA1GC present very similar MPSDs, which does not agree with the results obtained by CO_2 adsorption analysis (Figure 5), where the MPSD of sample KUA1B8 was much narrower than that of sample KUA1GC. This fact can be explained, as mentioned earlier, if we consider, once more, that HRTEM is detecting closed porosity existing in sample KUA1B8, which is not accessible to CO_2 adsorption. Thus, taking into account that CO_2 is only measuring the accessible porosity, the MPSD obtained by CO_2 adsorption for sample KUA1B8 must be much narrower than that of sample KUA1GC. On the other hand, in the case of HRTEM, the technique seems to be detecting both the open and the closed porosity, and because of that, the MPSD obtained for sample KUA1B8 is very similar to that for sample KUA1GC. These results make sense, considering that, as mentioned previously, sample KUA1B8 has been prepared by partially blocking the porosity of sample KUA1GC by cracking hydrocarbons.

These results indicate that HRTEM combined with image analysis is useful for structural analysis of narrow micropores, including closed porosity. To confirm that HRTEM is detecting closed porosity, further research is being carried out with other carbon molecular sieve materials, which have not been prepared by a cracking process. In these cases, the amount of closed porosity should be much lower, and then the MPSDs obtained by HRTEM should be more concordant with those obtained by CO_2 adsorption data.

Conclusions

The transfer function of the HRTEM was verified by comparing the power spectrum of the HRTEM image with the effective transfer function calculated logically. In view of this result, the measurement method by HRTEM and image analysis was applied to two activated carbons and a carbon molecular sieve, and the micropores, including the narrow micropores (ultramicropores), can be observed precisely.

The present work presents a useful comparison of two very different techniques: gas adsorption and image analysis of HRTEM micrographs. The MPSDs obtained by CO_2 adsorption and HRTEM demonstrated that both techniques give complementary results and can be used independently to characterize porous carbons, and especially CMSs, which are difficult to characterize with the well-established N_2 adsorption at 77 K. Thus, it has been shown that the MPSD obtained for a chemical activated carbon (sample KUA1GC) is concordant with that obtained from CO_2 adsorption. In addition, this technique has allowed us to obtain the MPSD of a carbon molecular sieve (sample KUA1B8), which could only be characterized by CO_2 adsorption at 273 K (not by N_2 adsorption at 77 K due to diffusional problems). The MPSD obtained by HRTEM for this sample is wider than that obtained by CO_2 adsorption, which suggests that HRTEM is detecting the closed porosity existing in this sample, which is not accessible to gas adsorption. To confirm this fact, further work is being carried out with other carbon molecular sieves that do not present closed porosity.

Thus, HRTEM combined with image analysis can be useful for structural analysis of narrow micropores including closed porosity.

Acknowledgment. The authors thank MCYT (Project No. PPQ2003-03884) for financial support. D.L.-C. thanks MEC for the postdoctoral grant. The support of the Japan Society for the Promotion of Science [work for "Japan−France Research Cooperative Programs" and for "the CLUSTER"] and of the Ministry of Education, Sports, Culture, Science and Technology of Japan [work partly supported by a Grant-in-Aid for Scientific Research (No. 14550311)] is gratefully acknowledged.

References and Notes

(1) Cazorla-Amorós, D.; Alcañiz-Monge, J.; Linares-Solano, A. *Langmuir* **1996**, *12*, 2820.
(2) Cazorla-Amorós, D.; Alcañiz-Monge, J.; De la Casa-Lillo, M. A.; Linares-Solano, A. *Langmuir* **1998**, *14*, 4589.
(3) Linares-Solano, A.; Salinas-Martínez de Lecea, C.; Alcañiz-Monge, J.; Cazorla-Amorós, D. *Tanso* **1998**, *185*, 316.
(4) Lozano-Castello, D.; Cazorla-Amoros, D.; Linares-Solano, A. *Carbon* **2004**, *42*, 1231.
(5) Lozano-Castello, D.; Cazorla-Amoros, D.; Linares-Solano, A.; Quinn, D. *J. Phys. Chem. B* **2002**, *106*, 9372.
(6) Lozano-Castelló, D.; Raymundo-Piñero, E.; Cazorla-Amorós, D.; Linares-Solano, A.; Müller, M.; Riekel, C. *Carbon* **2002**, 2727.
(7) Lozano-Castelló, D.; Raymundo-Piñero, E.; Cazorla-Amorós, D.; Linares-Solano, A.; Müller, M.; Riekel, C. *Characterisation of Porous Solids VI*; Studies in Surface Science and Catalysis; Elsevier: Amsterdam, 2002; p 51.
(8) Lozano-Castello, D.; Cazorla-Amoros, D.; Linares-Solano, A. *Chem. Eng. Technol.* **2003**, *26*, 852.
(9) Endo, M.; Furuta, T.; Minoura, F.; Kim, C.; Oshida, K.; Dresselhaus, G.; et al. *Supramol. Sci.* **1998**, *5*, 261.
(10) Endo, M.; Kim, Y. J.; Ishii, K.; Inou, T.; Nomura, N.; Mihashita, N.; Dresselhaus, M. S. *J. Mater. Res.* **2003**, *18*, 693.
(11) Endo, M.; Kim, Y. J.; Hayashi, T.; Oshida, K.; Miyazaki, T. *New frontiers in carbon materials*; Carbon 2003 Precongress Short Course; Alicante, Spain; p 33.
(12) Lozano-Castello, D.; Alcañiz-Monge, J.; Cazorla-Amoros, D.; Linares-Solano, A.; Zhu, W.; Kapteijn, F.; Moulijn, J. A. *Carbon* **2005**, *43*, 1643.
(13) Lozano-Castello, D.; Lillo-Rodenas, M. A.; Cazorla-Amoros, D.; Linares-Solano, A. *Carbon* **2001**, *39*, 741.
(14) Oshida, K.; Kogiso, K.; Matsubayashi, K.; Takeuchi, K.; Kobori, S.; Endo, M.; Dresselhaus, M. S.; Dresselhaus, G. *J. Mater. Res.* **1995**, *10*, 2507.
(15) Sharma, A.; Kyotani, T.; Tomita, A. *Carbon* **2000**, *38*, 1977.
(16) Huttepain, M.; Oberlin, A. *Carbon* **1990**, *28*, 103.
(17) Oshida, K.; Nakazaw, T. *Mem. Nagano Natl. College Technol.* **2000**, *34*, 40.